Title

Evaluating the use of rate-based monitoring for improved fatigue remnant life predictions

Authors

Leung, Michael Siu Hey
Corcoran, Joseph
Cawley, Peter
et al.

Publication Date

2019-03-01

DOI

10.1016/j.ijfatigue.2018.11.012

Peer reviewed

Evaluating the use of Rate-based Monitoring for Improved Fatigue Remnant Life Predictions

Leung, Michael[1], Corcoran, Joseph[1], Cawley, Peter[1], and Todd, Michael D.[2]

[1]Department of Mechanical Engineering, Imperial College London, UK

[2]Jacob School of Engineering, University of California San Diego, US

Abstract

The ability to perform accurate remnant life predictions is crucial to ensure the integrity of engineering components that experience fatigue loading during operation. This is conventionally done with periodic inspections, where results from non-destructive evaluation and estimation of the operating conditions are obtained to perform remnant life predictions using empirical crack growth laws. However, remnant life predictions made with this approach are very sensitive to their input parameters; uncertainty in each parameter would aggregate and result in great uncertainty in the final prediction. Recent technological advances have made permanently installed monitoring systems increasingly viable, making it possible to obtain and monitor trends in damage growth rate. It is proposed that the rate of damage growth can be used to more accurately and confidently gauge the integrity of an engineering component and perform remnant life predictions using the Failure Forecast Method. A statistical analysis of an example fatigue crack growth test was performed to compare the uncertainties of the remnant life predictions made using the conventional inspection approach, which utilises nominally-known operating conditions and empirical crack growth laws, and the proposed rate-based monitoring approach. Results show that the remnant life predictions made using the Failure Forecast Method produce significantly more accurate and confident predictions compared to the inspection approach. The Failure Forecast Method can also be adapted to accommodate load changes. An example fatigue test with a 20% load reduction after a period of crack growth was performed and the life predictions made with inspection data at the time of the load change and monitoring data up to that point were compared. Again it was shown that the uncertainty in the life prediction with the Failure Forecast Method using the monitoring data was lower than that with the inspection approach, but the improvement was smaller than in the constant load case because data on the load change and the Paris law exponent were required, thus increasing the uncertainty. The study has shown that the frequent data obtained from permanently installed monitoring systems provides new opportunities in remnant life estimates and potentially opens the way to increasing the intervals between outages and reducing design conservatism.

1 Introduction

Fatigue damage is considered to be one of the leading causes of failure in a range of engineering applications. Under cyclic loading, defects can initiate and propagate through engineering structures even when the loading results in stresses below its tensile strength [1]. This can lead to unexpected catastrophic failures that are costly to repair and potentially hazardous to operators and the public [2, 3, 4].

Conventionally, periodic in-service non-destructive evaluation (NDE) inspections of critical engineering components are performed to ensure components operate and degrade as expected. Components found to contain defects are assessed to estimate whether the defect would propagate under its operating conditions, and if so, perform remnant life predictions (RLPs) using empirical crack growth laws. This structural integrity assessment procedure would dictate whether the component is deemed safe to continue service or to necessitate repair or replacement.

Despite significant efforts in developing accurate models of fatigue crack growth, the predictions made by these models are very sensitive to uncertainties in input parameters, such as the measured defect geometry, material properties and loading conditions [5, 6]. Consequently, and since fatigue damage accumulation is stochastic in nature [7], greatly conservative estimates would have to be made to ensure the probability of failure is below standardised levels [8, 9].

With recent advances in technologies, on-line structural health monitoring (SHM) of engineering structures using permanently-installed monitoring systems (PIMS) become an increasingly viable solution to assess the structural health of engineering structures. On-line SHM can provide a continuous, real-time, estimate to how the actual component is responding to the actual operating conditions. Significant research is being conducted to develop technologies for on-line SHM of engineering components susceptible to fatigue damage. These include ways of monitoring the operating conditions of components [10], ways of detecting defect initiations such as vibration response monitoring [11] and acoustic emissions monitoring [12], or ways to monitor crack growth [13]. Previous literature has focussed on a natural extension to the conventional inspection based approach of using empirical crack growth or damage accumulation laws, but where crack length data is instead provided by SHM systems [14]. However, little research has been conducted to utilise the ability of PIMS to obtain continuous trends in damage growth rate for fatigue RLPs. Using PIMS, measurements can be made much more frequently compared to conventional inspections as illustrated in Figure 1 plotting the measured crack length of a fatigue experiment against the number of loading cycles. The red crosses are analogous to data obtained via regular in-service inspections, while the blue dots represent data that can be obtained with monitoring. The use of PIMS introduce the possibility of obtaining characteristic features of the rate of damage accumulation which can be used to perform RLPs.

Fatigue damage is an example of a positive feedback mechanism [15]; an increase in damage leads to an increase in the rate of damage accumulation as can be seen in Figure 1. Consequently, the fatigue crack growth rate behaviour has a characteristic form [15]. This behaviour was first noted by Voight [16], who subsequently developed the Failure Forecast Method (FFM), which utilises this characteristic form of damage accumulation rate to perform RLPs. Compared to conventional damage assessment methods, the FFM does not rely on assumptions of material properties, geometry, or operating conditions, but rather the observed response of the

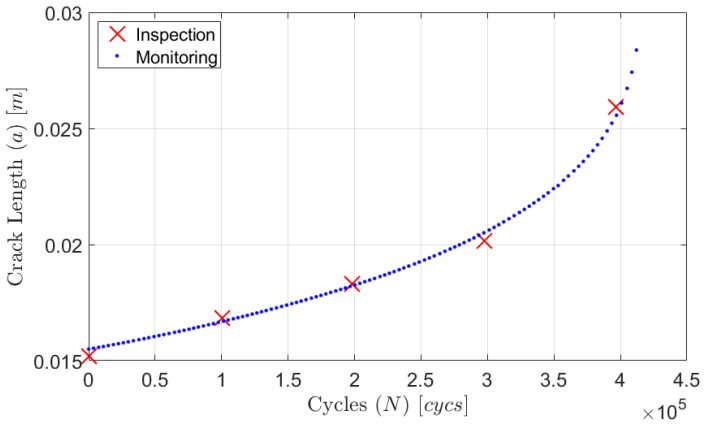

Figure 1: Plot of crack length against number of loading cycles for the fatigue experiment. The red crosses are analogous to data obtained via regular in-service inspections, while the blue dots represent what a PIMS can obtain.

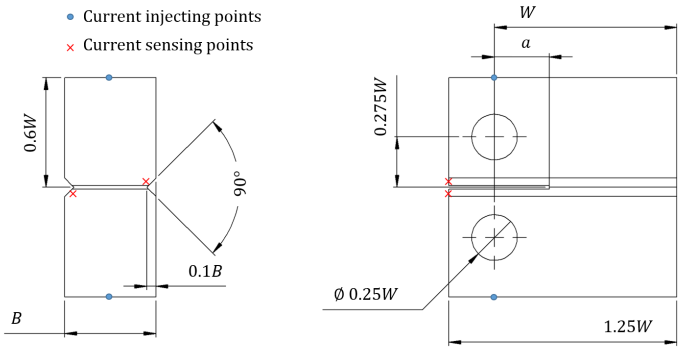

Figure 2: Geometry of the specimen used in the experiment

component. This reduces the number of sources of uncertainty and potentially provides more confident RLPs.

To demonstrate the advantages of using the rate-based monitoring approach to fatigue RLPs, a statistical analysis was conducted to establish the confidence of fatigue RLPs using both an inspection and monitoring approach. The analysis is conducted on crack growth data obtained from a fatigue experiment using a standard 316 stainless steel compact tension specimen; the geometry and loading parameters are given in Table 1 and Figure 2. The crack propagation is monitored using a permanently-installed potential drop measurement system, and the results plotting crack length as a function of number of loading cycles are shown in 1. The experiment is intended to represent a hypothetical example of where a defect is found on a component. The analysis aims to compare the confidence in the predictions made with both methods throughout the remnant life of the component after the defect is identified. The framework of the analysis can also be used as a tool in real-life applications to assess the confidence in predictions using the rate-based monitoring approach.

The paper begins by detailing the methodology of the inspection and monitoring approach to perform RLPs and subsequent uncertainty analysis based on Monte-Carlo simulation for the inspection approach and a specific uncertainty model developed for the regression-based implementation of the FFM as demonstrated in [18]. The two approaches are then used to analyse the example fatigue experiment. The accuracy and confidence in the predictions made by the two methods are then compared and discussed. A method of using the rate-based monitoring approach for variable amplitude fatigue is also proposed, validated and discussed.

Table 1: Geometry and loading parameters of the specimen in accordance to ASTM 647 [17] shown in Figure 2.

Parameter	Value
W (mm)	50
B (mm)	25
a (mm)	15.5
Maximum load, P_{max} (kN)	11
Load ratio, R	0.1

2 Inspection Approach to Remnant Life Predictions

2.1 Review of methodology

Using the conventional inspection approach, when defects are found with NDE inspections in an engineering component and sufficient information on the operating conditions, material properties and geometry of the component is available, empirical crack growth laws can be used to perform RLPs. There are many empirical crack growth laws available, the simplest being the Paris crack growth law [19], which is widely used to evaluate fatigue RLPs in real-life engineering applications across different industries [4, 8, 9]. The Paris law is given as,

$$\frac{da}{dN} = C(\Delta K)^m = C\big(Y(a)\Delta\sigma\sqrt{a}\big)^m \tag{1}$$

where C and m are material constants known as the Paris' constant and exponent respectively;ΔK is the stress intensity range as a result of stress range, $\Delta\sigma$, and crack length, a; $Y(a)$ is the geometry function as a function of crack length. Integrating from the initial crack length, a_0 to the failure crack length, a_f gives,

$$N_f = \int_{a_0}^{a_f} C^{-1}\big(Y(a)\Delta\sigma\sqrt{a}\big)^{-m} da \tag{2}$$

where N_f is the remnant life prediction of the component.

As with many other modes of material failure, fatigue damage accumulation is by nature probabilistic, hence probabilistic methodologies are needed to quantify uncertainties and determine the level of conservatism required [7, 20]. A regularly-inspected component is deemed safe for continued operation if the probability of failure of the component is kept below a predefined threshold up to the next scheduled inspection. A reconstructed schematic of how inspections update the probability of failure from DNVGL-RP-C210 is shown in Figure 3 [9]. If the probability of failure exceeds a critical value prior to the next scheduled inspection, its integrity would no longer be guaranteed, and actions will need to be taken to repair or replace the component. The critical probability of failure of the component is specific to each engineering application, mainly dictated by the risks and consequences involved should a failure occur.

As a result, confidence in RLPs are crucial to minimise conservatism and hence make it possible to safely operate the component closer to its actual failure time. To evaluate the confidence in the RLPs made, the uncertainties for all individual parameters will have to be quantified for the analysis as detailed in Table 2. A discussion on quantifying these values is given below.

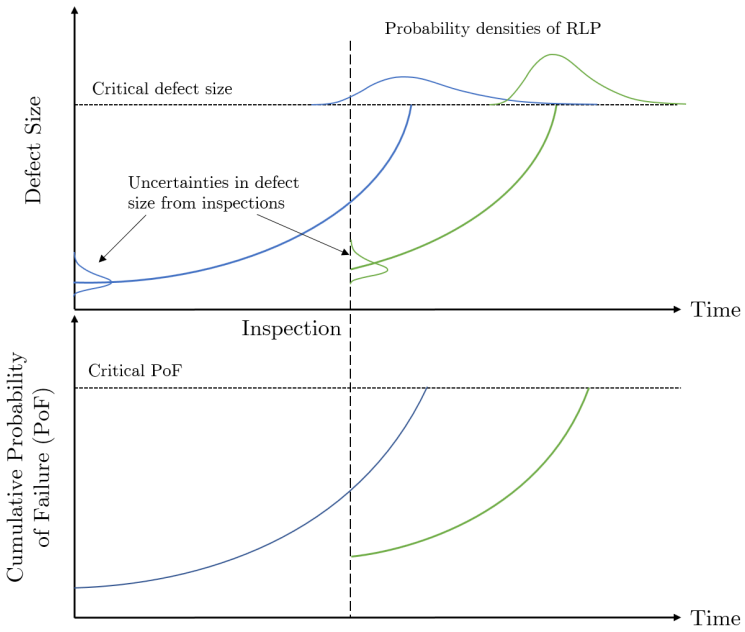

Figure 3: Schematic reconstructed from the DNVGL Recommended Practice C210 showing how the probability of failure updates with an inspection [9].

Since crack growth in only one direction is considered in this analysis, the geometry of the defect can be characterised by a single crack length measurement, a_0. This measurement is updated every time an inspection is conducted. The error in defect size measured from NDE is assumed to be normally distributed with a standard deviation of 1 mm and no bias. This greatly depends on the NDE technique used as well as positioning and geometry of the defect. Other than the capabilities of the NDE technique, there are also other sources of uncertainties, such as the placement of measurement probes as well as calibration error [21]. The assumption made here is optimistic and is approximated with the nominal capabilities of a state-of-the-art NDE system [22].

The critical crack length a_f is often conservatively estimated from the plane strain fracture toughness of the component using linear elastic fracture mechanics. The uncertainty in this is not considered for the analysis as the final crack length has a relatively small effect on the final estimated failure cycle.

The Paris constant C and exponent m of a specific component are very rarely known with accuracy as they can vary even with the same material under nominally identical conditions as demonstrated by Virkler [5]. The constants are typically fitted retrospectively to fatigue test data to capture the stochastic nature and material variability, and hence exact values are unavailable for RLPs. Standardised values and standard deviations of the constants from the British Standards 7910 [8] as shown in Table 2 are therefore used to simulate how analyses are typically done in real-life.

The operating conditions of the component include loading cycles experienced, temperature of the environment and the effect of aggressive environments, all of which could have an effect on the crack growth characteristics. Only the nominal stress range $\Delta\sigma$ is considered in this analysis. The error in loading is assumed to be normally distributed with a standard error of $3.5kN$ (10% of the maximum load) and no bias. The error in load ratio, R, is not considered. Again, an optimistic assumption is made here as the uncertainty in loading is highly dependent on the application and whether design load or loading data based on on-line SHM is used.

Table 2: Table showing the quantified uncertainties of each input parameter of the empirical crack growth law

Parameter	Mean value	Standard error
Measured crack length, a_0 (mm)	Updates with each inspection	1
Critical crack length, a_f (mm)	38	not considered
Paris constant, $ln(C)$	-25.5	0.264
Paris exponent, m	2.88	not considered
Maximum load, P_{max} (kN)	35	3.5
Load ratio, R	0.1	not considered
Geometry, $Y(a)$	Calculated from standards	not considered

It is fully recognised that the assumptions made on the statistical variation of the input parameters are hugely simplistic; the uncertainty of the parameters are assumed to be independent, and the effect of uncertainty in geometry is not considered. However, it is believed that these assumptions are sufficient to illustrate the effect of how uncertainties of each input parameter aggregate to result in significant uncertainties in the RLP. The assumptions made here are optimistic and greater uncertainties are to be expected in real-life as mentioned above. This method offers a framework that may be used for the analysis of more specific examples.

2.2 Statistical Analysis on Remnant Life Predictions

Incorporating all these uncertainties, a 10,000-trial Monte-Carlo simulation was performed to evaluate the probability density function (PDF) of the remnant life of the component described earlier. All the input parameters are sampled randomly from their statistical distributions defined in Table 2 and kept constant for each trial, and the predicted N_f is calculated using Equation 2. A log-normal distribution was then fitted to the simulation results to obtain statistical properties of the prediction [5].

The PDF of the predicted N_f prior to the experiment ($N = 0$, where N is the number of loading cycles the component has experienced) is plotted in Figure 4. The point at which failure occurred during the experiment is shown with a dotted black line, which is at $4.24 \times 10^5 cycs$. From the results of the analysis the confidence in the predicting remnant life can be quantified. The 3σ lower and upper confidence bounds at the beginning of the experiment were 2.10×10^5 *cycs* and 2.26×10^6 *cycs* respectively, showing that the confidence in the predicted N_f is rather low, with a 3σ confidence interval that spans over an order of magnitude. As previously discussed, it is necessary to adopt the lower bound estimate as the RLP to ensure conservative operation; large uncertainty therefore requires extreme conservatism.

The PDF can be updated with each inspection as shown in Figure 5. In this case, it is assumed that an inspection was performed every 10^5 *cycs*. As seen from the results in this particular case, the inspection-based approach is initially overestimating N_f, gradually converging to the actual N_f with each inspection being closer to failure.

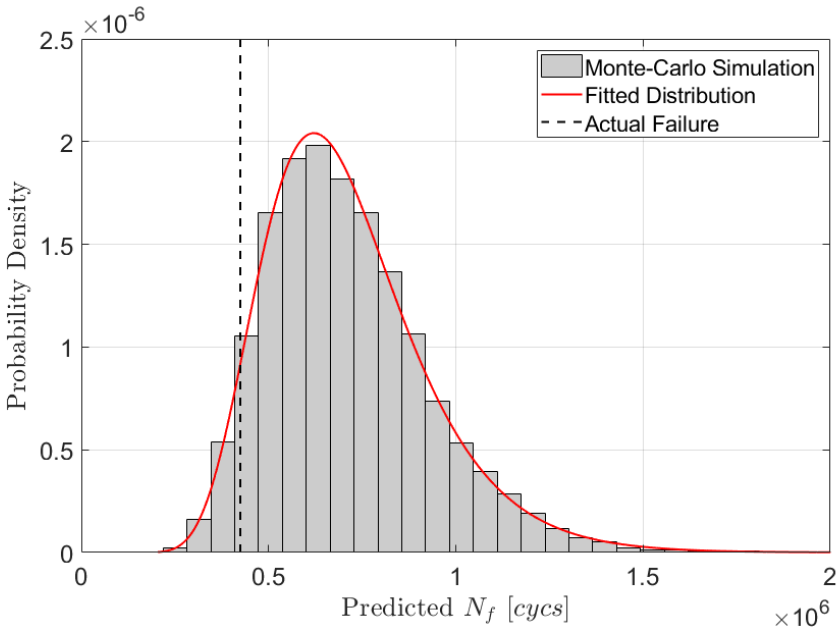

Figure 4: Results of the Monte-Carlo simulation to obtain the probability density function of the failure cycle at $N = 0$. The dotted black line indicates the actual failure time of the experiment, $N_f = 4.24 \times 10^5 cycs$.

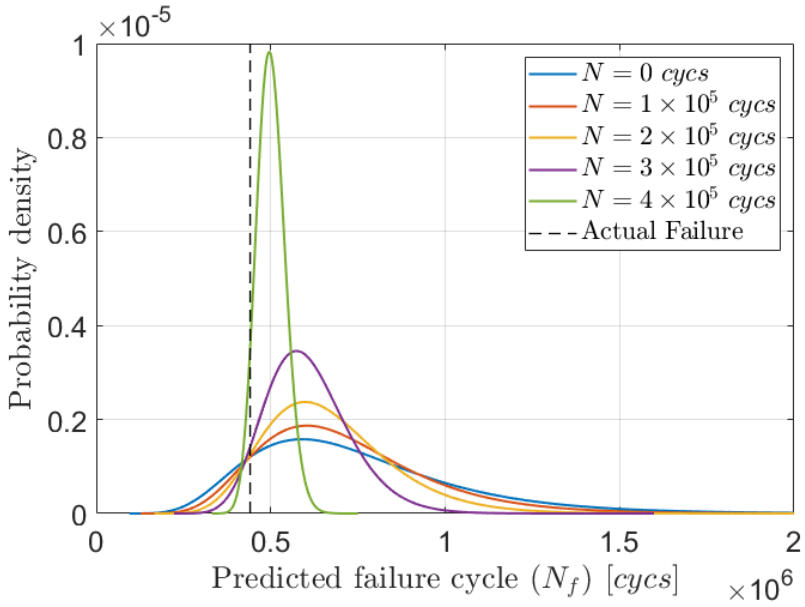

Figure 5: Fitted distribution of predicted failure cycle at every 10^5 $cycs$.

3 Monitoring Approach to Remnant Life Predictions

An alternative way of performing RLPs is the monitoring approach. Instead of conducting periodic in-service inspections, a PIMS can be installed to monitor the rate at which the damage accumulates. RLPs can then be performed in real-time while the component is in operation using the Failure Forecast Method (FFM).

3.1 Review of Methodology

Voight first observed that the relationship,

$$\Big(\frac{d\Omega}{dt}\Big)^{-\alpha}\Big(\frac{d^2\Omega}{dt^2}\Big) - A = 0 \tag{3}$$

can be used to describe rate-dependent material failures such as fatigue crack growth, where Ω is an observable metric of damage and α and A are arbitrary constants [23]. He proceeds to state that the equation can be integrated for $\alpha > 1$ to give,

$$\left(\frac{d\Omega}{dt}\right)^{1-\alpha} = A(\alpha-1)(t_f - t) + \left(\frac{d\Omega}{dt}\Big|_f\right)^{1-\alpha} \tag{4}$$

where t_f is the failure time and $\frac{d\Omega}{dt}\big|_{f'}$ is the rate of damage accumulation at failure.

The rate of damage accumulation at failure is often orders of magnitude greater than accumulation rates early on in fatigue life. It is therefore reasonable to assume that the rate of damage accumulation at failure to be infinite. Also, it is observed that for many cases including fatigue crack growth, $\alpha \approx 2$. A more detailed discussion on this by Corcoran can be found in [15]. Hence, applying the above assumption and putting Equation 4 in the context of fatigue crack growth as a function of loading cycles, N, we get,

$$\Big(\frac{d\Omega}{dN}\Big)^{-1} = A(N_f - N) \tag{5}$$

so,

$$N_f = N + \frac{1}{A}\Big(\frac{d\Omega}{dN}\Big)^{-1} \tag{6}$$

where Ω now becomes a measurable quantity that changes with crack growth. This can be any output signal from existing NDE techniques that share the same characteristic response of the damage accumulation mechanism [15].

Using Equation 5, the failure cycle, N_f, can be estimated by performing a regression analysis on the inverse damage accumulation rate, $\dot{\Omega}^{-1}$ against the number of loading cycles, then extrapolating the regression fit and finding the x-axis intercept where crack growth rate is infinite as demonstrated in Figure 6. By assuming $\alpha = 2$ such that the regression becomes linear, the RLP would be the negative ratio between the intercept and slope of the regression fit. This method of performing RLPs is known as the Failure Forecast Method (FFM).

To demonstrate the use of the FFM for RLPs, the experimental results were analysed using the method, simulating a PIMS being installed on the defective component while it continues operation. The rate of change in

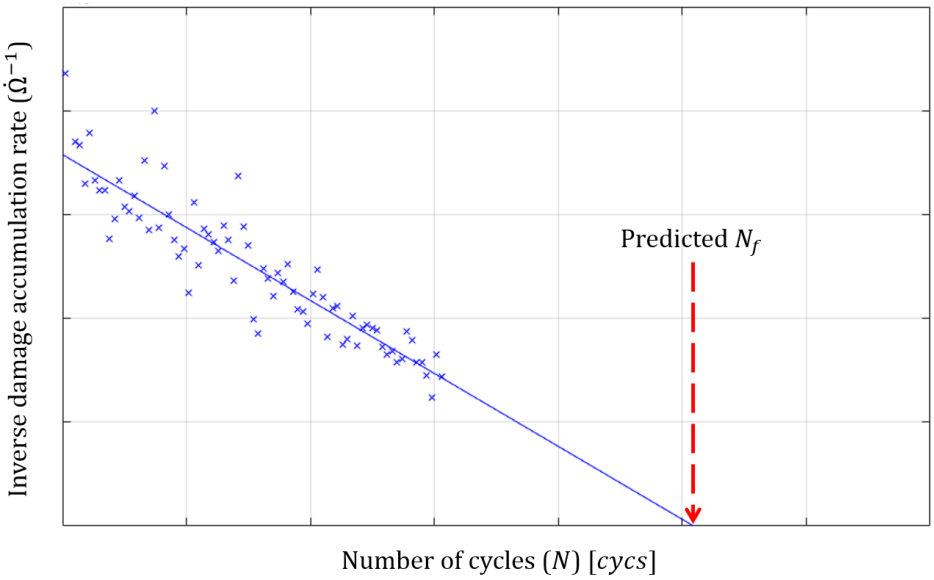

Figure 6: Illustration of inverse damage accumulation rate ($\dot{\Omega}^{-1}$) against number of cycles for a set of fatigue testing data to schematically demonstrate the use of the FFM for RLPs.

signal, in this case the resistance measurement, R, from the potential drop measurement system, is calculated to perform the FFM analysis without converting to crack length measurements as with typical analysis of potential drop measurement results. This is obtained from the slope of the linear regression fit performed on every 5 resistance measurements. The inverse of the rate of change in resistance, $\dot{R}^{-1}$, is then calculated and a linear regression analysis of the data is performed to obtain the predicted N_f. Figure 7 plots the results in intervals of 10^5 *cycs*. In this analysis, the most recent 100 $\dot{R}$ data points were used as indicated on the plot by the two red lines. The dotted black line indicates the actual failure cycle. Predictions are made in real time as the component is fatigued, with the plot of predicted N_f against number of fatigue cycles shown in Figure 8; again, the dotted line is where actual failure occurred.

Utilising an on-line PIMS that takes frequent measurements and hence provide continuous rate estimates, the predicted N_f can be continuously updated as more damage accumulation rate data is obtained in-service to provide real-time RLPs. The major advantage of using the FFM for RLPs is that minimal knowledge on the operating conditions is required. As opposed to RLPs made with inspection results, parameters including loading conditions, material properties, geometry of the component and actual crack length measurements are not required. Assuming that all operating conditions remain constant, the only input required for the FFM is any input signal that can be used to measure the rate of damage accumulation.

3.2 Statistical Analysis of Remnant Life Predictions

As opposed to the inspection approach where empirical crack growth laws are used, the FFM simply uses the extrapolated point of infinite damage accumulation rate as the predicted failure time. Therefore, the only source of random uncertainty for the FFM is the random uncertainty in the damage accumulation rate measurements, which in turn results in uncertainties in the regression fit and the extrapolated x-axis intercept.

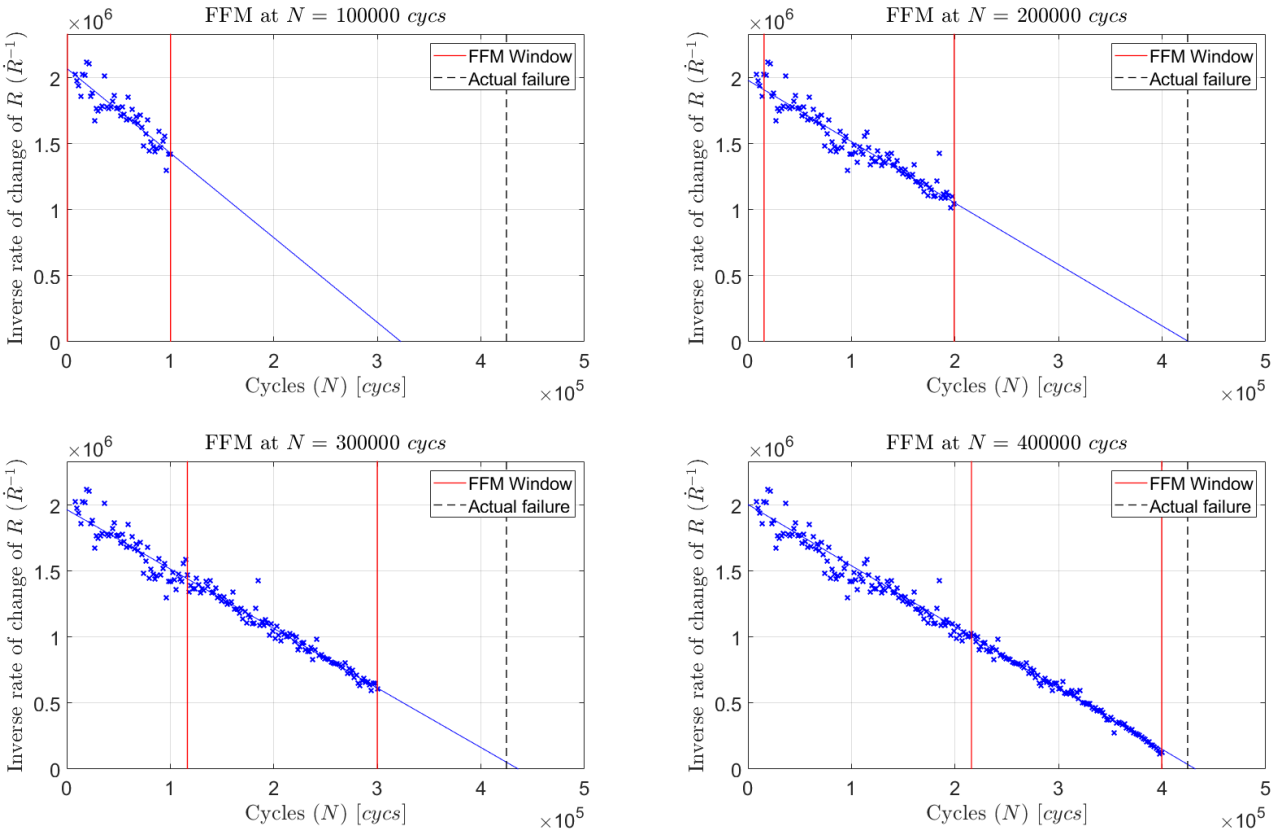

Figure 7: RLPs made using the FFM at intervals of $100,000$ *cycs*. The red line indicates the window of $\dot{R}$ data used for the FFM, and the dotted black line indicates the actual failure cycle.

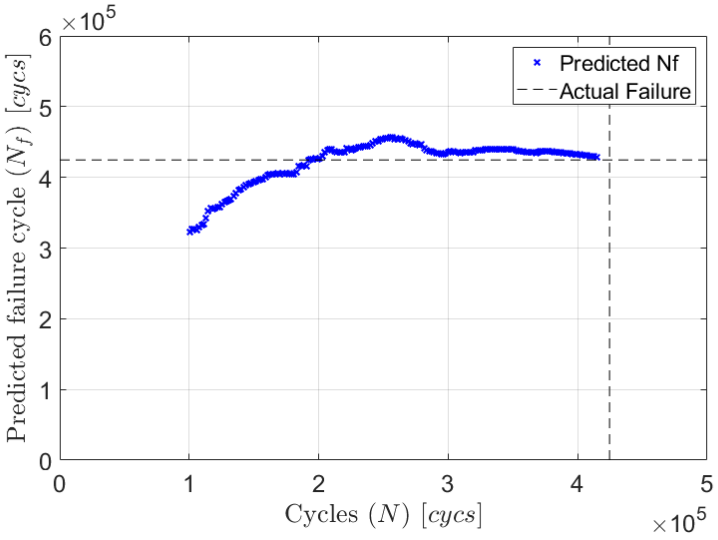

Figure 8: Plot of predicted N_f against number of loading cycles for the fatigue experiment

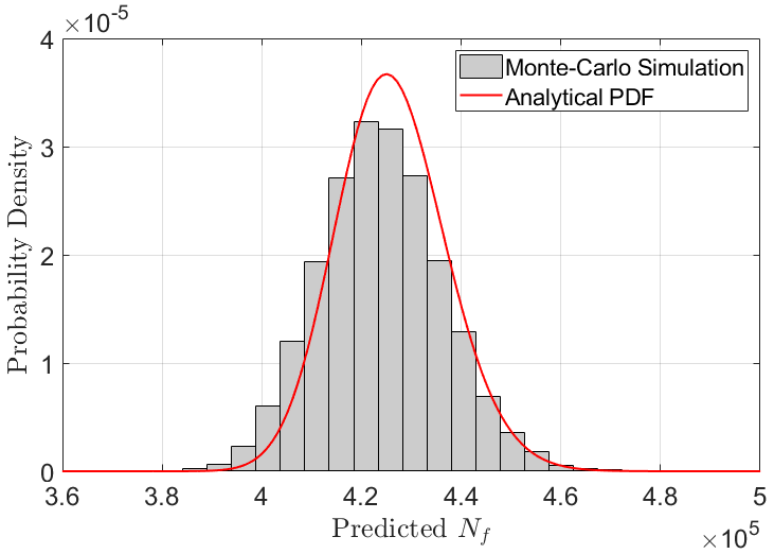

Figure 9: Plots of the PDF of the predicted failure cycle at 2×10^5 *cycs*. The grey bars represent the results of the Monte-Carlo simulation, the red graph represents the analytical solution.

The distribution of the predicted failure cycle, $p(\hat{N}_f)$, can be analytically evaluated as demonstrated by Todd et al [18]. The analytical solution is,

$$p(\hat{N}_f) = \frac{\sqrt{1-\rho^2}\sigma_0\sigma_1 e^{\frac{-\mu_1^2\sigma_0^2+2\rho\mu_0\mu_1\sigma_0\sigma_1-\mu_0^2\sigma_1^2}{2\sigma_0^2\sigma_1^2(1-\rho^2)}}}{\pi(\sigma_0^2+2\rho\sigma_0\sigma_1\hat{N}_f+\sigma_1^2\hat{N}_f^2)} + \frac{e^{\frac{(\mu_0+\mu_1\hat{N}_f)^2}{2(\sigma_0^2+2\rho\sigma_0\sigma_1\hat{N}_f+\sigma_1^2\hat{N}_f^2)}} erf\left[\frac{\mu_0\sigma_1(\rho\sigma_0+\sigma_1\hat{N}_f)-\mu_1\sigma_0(\sigma_0+\rho\sigma_1\hat{N}_f)}{\sqrt{2-2\rho^2}\sigma_0\sigma_1\sqrt{\sigma_0^2+2\rho\sigma_0\sigma_1\hat{N}_f+\sigma_1^2\hat{N}_f^2}}\right]\left(\mu_0\sigma_1(\rho\sigma_0+\sigma_1\hat{N}_f)-\mu_1\sigma_0(\sigma_0+\rho\sigma_1\hat{N}_f)\right)}{\sqrt{2\pi}(\sigma_0^2+2\rho\sigma_0\sigma_1\hat{N}_f+\sigma_1^2\hat{N}_f^2)^{3/2}} \tag{7}$$

where:

- $erf(*)$ = the error function;
- $\hat{N}_f$ = variable for the predicted failure cycle
- μ_j = mean estimate of the intercept and slope, denoted with subscript 0 and 1 respectively
- σ_j = estimated standard deviation of the intercept and slope, denoted with subscript 0 and 1 respectively
- ρ = correlation coefficient of the intercept and slope of the linear regression

The PDF can be obtained in real time to estimate the confidence in the RLPs made using the FFM and updated when new data points are obtained while the component is in operation. The results were verified with a Monte-Carlo simulation using synthetic data with random measurement uncertainties characterised by the actual data set from the experiment. The results at $N = 2 \times 10^5$ *cycs* for both the analytical and 10000-trial Monte-Carlo simulation is shown in Figure 9. For better comparison with the inspection results which are plotted in blue, only the results for every 10^5*cycs* is plotted in Figure 10.

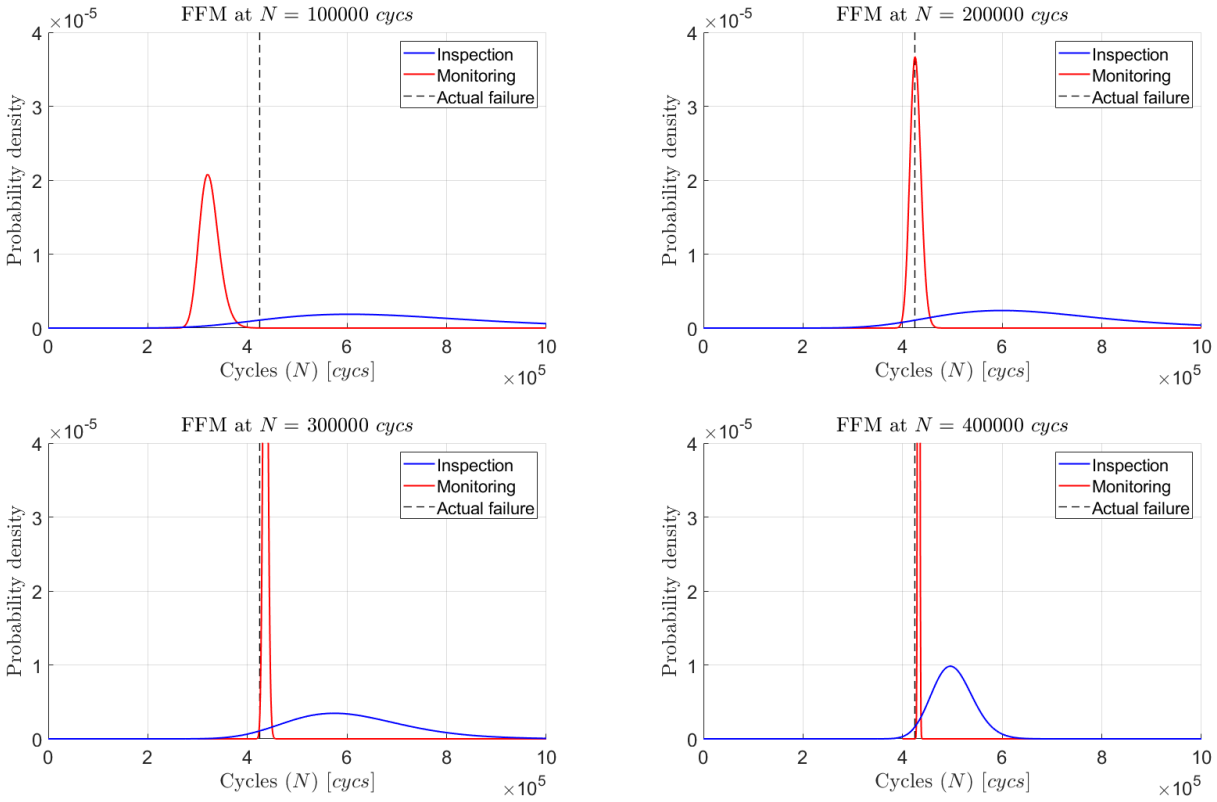

Figure 10: Plots of the PDF of the predicted failure cycle at intervals of $100,000$ *cycs*. The blue graph represents the inspection approach, the red graph represents the monitoring approach, the dotted black line is when the component failed.

4 Comparing the Inspection Monitoring Approach to Fatigue RLPs

4.1 Statistical Comparison between Inspection and Monitoring

Figure 11 plots the median RLPs of the inspection and monitoring results, showing that the RLPs made using the monitoring approach convergences much more quickly to the actual failure cycle. From 2×10^5 *cycs* onwards, approximately half the life of the component, all predictions made using the monitoring approach were within 10% the actual failure cycle. Conversely with the inspection approach, there is no way of adapting or correcting for the actual operation conditions. With each inspection, only the measured crack length can be updated, while no additional information on the loading conditions and material properties can be obtained. Therefore, the RLPs made converges slowly to the actual failure time as the end of life of the component approaches.

Not only are the RLPs more accurate with the monitoring approach, the confidence in the RLPs made is significantly greater as shown in Figure 10. Consider the RLPs made with both methods at 2×10^5 *cycs*. Assuming that the target level of confidence in the integrity of the component is 99.7% (3σ), the conservative RLP using the inspection and monitoring approach would be $2.8 \times 10^5 cycs$ and 3.5×10^5 *cycs* respectively. At this point, the estimated remnant useful life of the component would be $0.8 \times 10^5 cycs$ should the inspection-based approach be used, while with the use of the monitoring-based approach, the component would have an estimated remnant useful life of 1.5×10^5 *cycs*. Given that an inspection is only performed every $10^5 cycs$, the component would fail to meet the required threshold of confidence in integrity before the next inspection. In comparison,

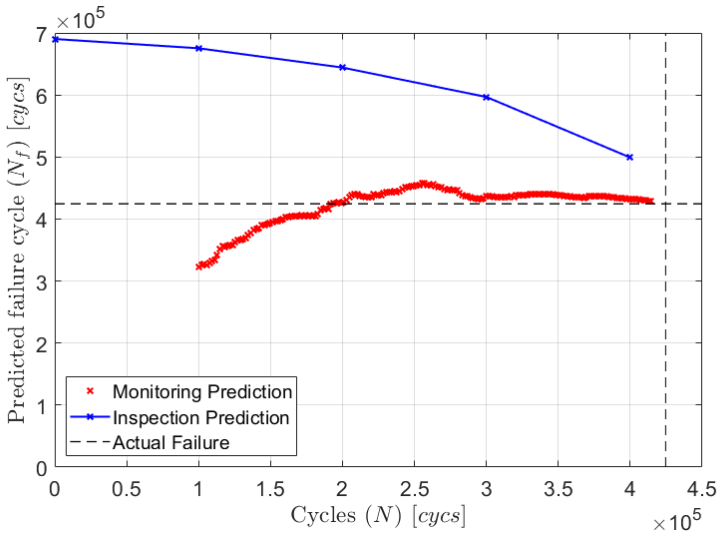

Figure 11: Plot of RLPs against number of loading cycles for both the inspection and monitoring approach.

due to significantly greater confidence, the conservative RLP made with the monitoring approach is much closer to the actual failure cycle.

While the choices of target confidence and inspection interval here are arbitrary, the study demonstrates how estimations with greater confidence via the monitoring approach make it possible to safely operate the component closer to its actual failure time. These predictions, including the confidence bounds, can be made in real time while the component is in operation. Thus, the use of monitoring can provide improved awareness of the damage state of the component without the need of inspections, potentially reducing the duration or even the frequency of costly planned outages.

4.2 Validity of using the FFM for Fatigue RLPs

Despite the RLPs made using the FFM having lower uncertainty, systematic errors resulting in bias in the RLPs are also apparent at various stages of the experiment. Even though the predictions are consistent and close to the actual failure time, the results in Figure 11 show that there is a consistent overestimation in the predictions made using the monitoring approach starting from approximately $2 \times 10^5 cycs$. There is also a clear underestimation of the remnant life during the initial cycles, even when the confidence in the predictions is considered.

The FFM assumes that the damage accumulation mechanism is constant throughout the life of the component. This assumption is not fully accurate as multiple stages of fatigue crack growth exist. Figure 12 (a) shows a typical schematic plot of crack growth rate against stress intensity factor, which is a function of stress, crack length and geometry of a fatigued component. Figure 12 (b) schematically shows how the subsequent plot of inverse crack growth rate against number of cycles would appear. This non-linear relationship between the inverse crack growth rate and number of cycles is believed to be the major cause of systematic error in the predictions made by the FFM. The systematic error in this experiment is however not very significant as the specimen of this test spends most of its fatigue life within the stage II crack growth regime.

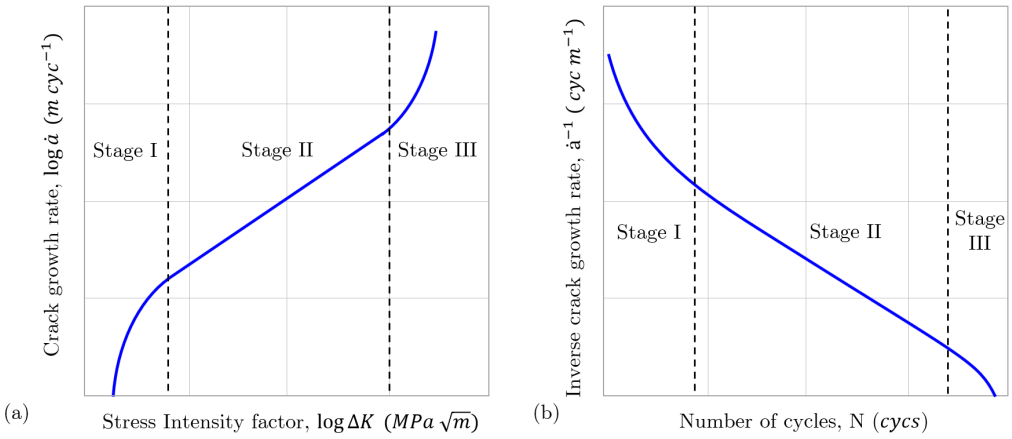

Figure 12: (a) Schematic plot of crack growth rate against stress intensity factor, which is a function of stress, crack length and geometry of a fatigued component; (b) resulting plot of inverse crack growth rate against number of cycles.

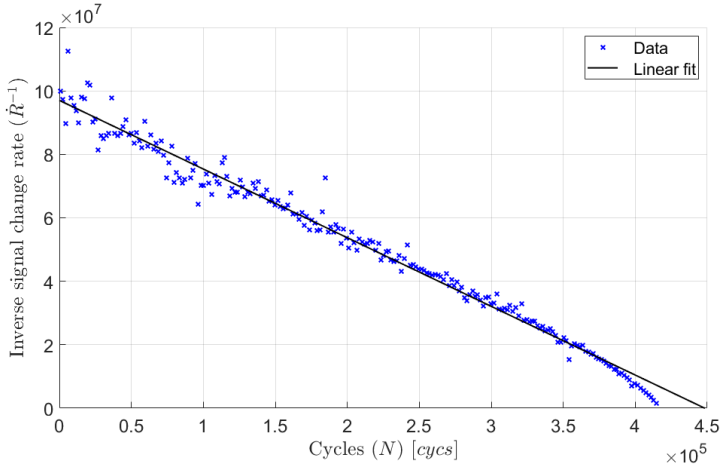

Figure 13: Plot of inverse crack growth rate against number of cycles, highlighting how the change in crack growth rate deviates from the linear relation at terminal stages of fatigue crack growth.

The crack growth mechanism is different during initial cycles of fatigue, since the radius of a fatigue crack tip is orders of magnitude smaller than the starter crack that was electrical discharge machined (EDM). Therefore, a fatigue crack would have to "initiate" from the EDM crack. This would have crack growth characteristics that in some ways resemble the stage I crack growth region; remnant life is thus underestimated as the slope of the regression fit of inverse crack growth rate against number of cycles is greater in stage I than in stage II crack growth.

The subsequent overestimation of remnant life can also be explained similarly. During the terminal stages (Stage III) of crack growth, the crack growth rate accelerates and deviates from the linear relationship between crack growth rate and stress intensity factor. This is also reflected in the plot of inverse crack growth rate against number of cycles as demonstrated in Figure 13, resulting in the component failing earlier than predicted by the FFM. A linear fit is plotted to better illustrate the acceleration in crack growth, which can be seen at around 4×10^5 *cycs*. However, since this terminal stage of fatigue crack growth is only a very small portion of the overall life of the component, the resulting overestimation is minimal.

It is therefore clear that for the FFM to provide accurate fatigue RLPs, the remnant fatigue life of the component

must be dominated by a single damage accumulation mechanism. In the case of this experiment, a majority of the fatigue life of the component is spent at Stage II, Paris law crack growth. Thus, the RLPs made in this region were accurate with relatively small systematic error. Such an error also exists with the inspection approach, but since there are such great uncertainties in the RLPs, its effect becomes negligible. More advanced empirical crack growth laws such as the Forman equation [24] or the NASGRO equation [25] can be used to better model the crack growth behaviour across multiple stages of fatigue crack growth. However, more input parameters, each with an associated uncertainty, is required for these crack growth laws, resulting in significant uncertainties in the prediction despite the crack growth model being accurate.

4.3 Failure Criterion of the FFM

As shown earlier in Equation 4 and 5, it was assumed that the damage accumulation rate at failure is infinite, hence the x-axis intercept of the plot of inverse growth rate against number of cycles is the estimated point of failure. This proves to be a valid assumption as shown in Figure 13 where the last data point is very close to the x-axis. The validity of this assumption is determined by the requirement that the period of monitoring would need to cover a significant fraction of the crack propagation life of the component such that the range of crack growth rates measured is sufficiently large.

In real-life engineering applications, there are cases where the failure criterion is instead determined by the ability of the component to withstand a critical load. An example of this would be the ability of an offshore wind turbine structure to withstand loads under extreme weather conditions [26], where failure under nominal loading conditions is no longer the failure criterion for the fitness of service of the component, as assumed with the FFM.

One potential way to accommodate this while using the FFM to perform RLPs is to introduce a finite critical crack growth rate failure criterion. With knowledge of the material properties of the component under its operating conditions as well as the correlation between stress intensity and crack growth rate, a maximum allowable crack growth rate using empirical crack growth laws can be obtained, as schematically demonstrated in Figure 14. The failure is then estimated to occur at the point where the linear regression of the FFM crosses a specific value of inverse crack growth rate instead of the x-axis intercept. However, this process requires more information on the materials properties and operating conditions, as well as a calibrated conversion between signal change and crack growth rate. This means that the advantage of using the FFM is significantly reduced as more information and thus uncertainties are introduced.

5 The Failure Forecast Method for Variable Amplitude Loading

Real-life engineering components are often subjected to varying loading conditions that cannot be simplified to a constant-loading fatigue problem. For example, if a defect is found in a power station component it is common to derate the unit to reduce the stress and so extend the component life. In this section, a method of compensating for the change in loading while using the FFM is proposed.

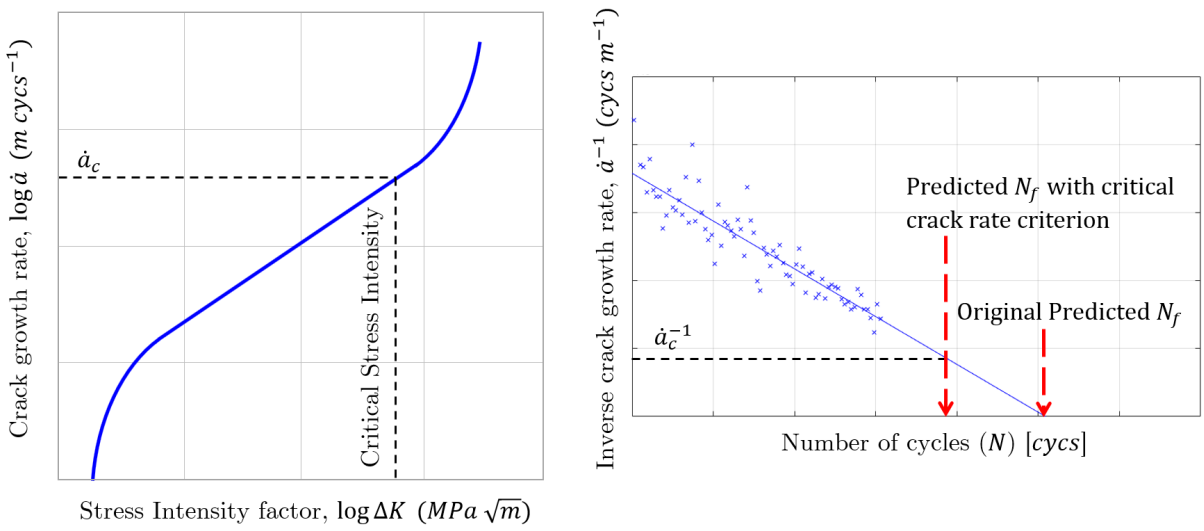

Figure 14: Schematic demonstration of how a finite critical crack growth rate can be introduced in the FFM.

5.1 Background Theory

Voight briefly outlined an expanded version of the integrated form of his equation to account for variable stresses at failure [23]. For $\alpha > 1$,

$$\frac{d\Omega}{dt} = \left(A(\alpha - 1)(t_f - t) + \left(\frac{d\Omega}{dt}\Big|_f \left(\frac{\sigma}{\sigma'} \right)^n \right)^{1-\alpha} \right)^{\frac{1}{1-\alpha}} \tag{8}$$

where σ' is some reference stress, σ is the actual stress at failure, and n is an empirical constant.

It is proposed that the above equation can be expressed in a more useful form by introducing the variables,

$$t_{eq} = t \times \left(\frac{\sigma}{\sigma'} \right)^{n(\alpha-1)}, \qquad t_{eq,f} = t_f \times \left(\frac{\sigma}{\sigma'} \right)^{n(\alpha-1)} \tag{9}$$

Substituting Equation 9 into Equation 8, rearranging and assuming infinite growth rate at failure, we get,

$$\frac{d\Omega}{dt_{eq}} = \left(A(\alpha - 1)(t_{eq,f} - t_{eq}) \left(\frac{\sigma}{\sigma'} \right)^{n(\alpha-1)(\alpha-2)} \right)^{\frac{1}{1-\alpha}} \tag{10}$$

Putting this in context of fatigue crack propagation,

$$\frac{da}{dN_{eq}} = \left(A(\alpha - 1)(N_{eq,f} - N_{eq}) \left(\frac{\Delta\sigma}{\Delta\sigma'} \right)^{n(\alpha-1)(\alpha-2)} \right)^{\frac{1}{1-\alpha}} \tag{11}$$

where,

$$N_{eq} = N \times \left(\frac{\Delta\sigma}{\Delta\sigma'} \right)^{n(\alpha-1)}, \qquad N_{eq,f} = N_f \times \left(\frac{\Delta\sigma}{\Delta\sigma'} \right)^{n(\alpha-1)} \tag{12}$$

This definition of equivalent cycles is similar to Basquin's exponential law for fatigue, which states that there is a power law relationship between the fatigue life of a component and the loading amplitude the component experiences [27]. What is shown here is that a similar relation can be used in crack growth monitoring and FFM

Table 3: Geometry and loading parameters of the variable-amplitude fatigue testing specimen in accordance to ASTM 647-15e1 [17] as shown in Figure 2.

Parameter	Value
W (mm)	80
B (mm)	20
a (mm)	16
Maximum load, P_{max} (kN)	35 kN for the first 4×10^4 cycles, then 28 kN until failure
Load ratio, R	0.1

to compensate for variable amplitude effects. It is also observed that the empirical constant n should equate to the Paris' exponent m. Assuming linear-elastic fracture mechanics, the Paris law is,

$$\frac{da}{dN} = C(\Delta K)^m = C\big(Y(a)\Delta\sigma\sqrt{a}\big)^m \tag{13}$$

It can be seen that the crack growth rate is proportional to the stress range raised to the power of m, hence it would be reasonable to assume that the two empirical constants are equal.

As mentioned earlier, it is reasonable to assume $\alpha = 2$. Therefore, Equation 11 simplifies to,

$$\Big(\frac{da}{dN_{eq}}\Big)^{-1} = A(N_{eq,f} - N_{eq}) \tag{14}$$

This is identical to Equation 5, that was used for the FFM analysis in previous sections, but with equivalent cycles replacing the actual cycles of loading. This shows that by introducing the definition of equivalent cycles N_{eq}, continuity of relation between the crack growth rate and number of cycles can be retained despite changes in loading amplitudes. Thus, the same method as discussed in Section 3 can be used to perform fatigue RLPs for variable amplitude fatigue, given that the relative change in loading, $\frac{\Delta\sigma}{\Delta\sigma'}$, and the Paris' exponent m are both known.

5.2 Variable Amplitude Fatigue Experiment

To validate the equivalent cycles method, a variable amplitude fatigue experiment using a CT specimen made of S275 steel with parameters shown in Table 3 was conducted while crack growth was monitored using the front-face compliance method using clip gauges. The experiment simulates the case where it is proposed that a defective engineering component is to be operated at derated conditions to limit the crack growth rate and it is necessary to predict the remnant life given the new loading. In this example, the maximum load is reduced by 20% while the load ratio remains constant. The experiment compares the accuracy and confidence in the RLPs made in the following two cases. The first case is where no PIMS was used, so an inspection to measure the crack length is conducted immediately prior to the derating to estimate the remnant life of the component. The second case is where a PIMS was installed on the component long before the derating, hence the FFM with the equivalent cycles method can be used to estimate the remnant life of the component using previously-collected data.

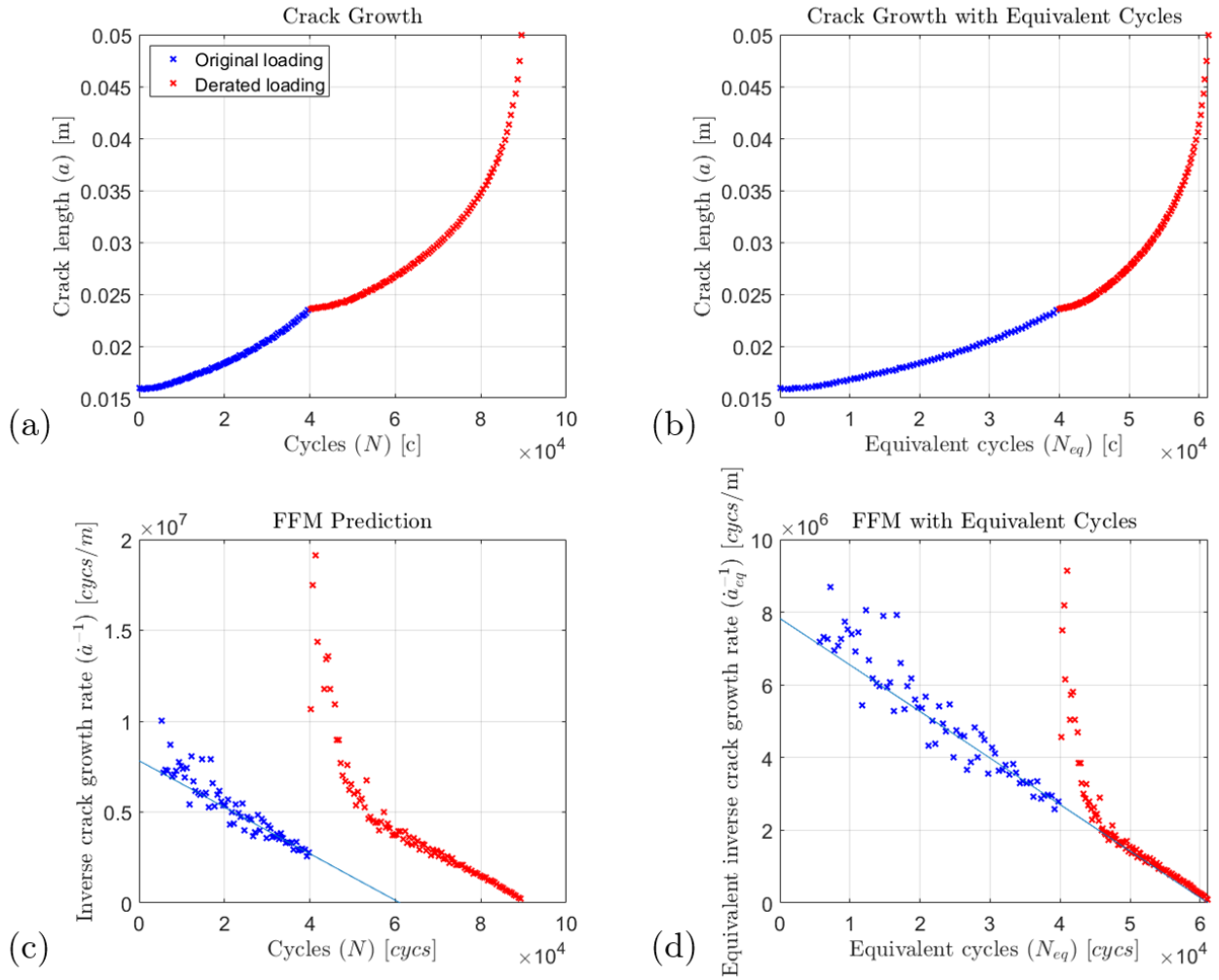

Figure 15: Plot of (a) crack length against number of cycles; (b) crack length against number of equivalent cycles; (c) inverse crack growth rate against number of cycles; (d) inverse crack growth rate against number of cycles for the variable amplitude fatigue experiment.

A plot of crack length against the number of cycles of the experiment is shown in Figure 15 (a). The blue and red data points represent measurements before and after the change in loading respectively; the blue data is used to make the prediction while the red data is included to show the experiment results. Figure 15 (c) and (d) show the inverse crack growth rate against number of cycles and equivalent inverse crack growth rate against equivalent number of cycles respectively. The use of the equivalent cycles method in Figure 15 restores the continuity of the plot of inverse crack growth rate against cycles, allowing for the use of FFM for fatigue failure analysis where the loading is not at constant amplitude. The FFM regression fits shown on the graphs were obtained using data collected from the first 4×10^4 cycles before the reduction in loading. Note that inverse crack growth rate is used only because calibrated measurements of crack length were readily accessible with this monitoring system. Should a different monitoring system be used, conversion from signal change to growth rate is not necessary.

To quantify the accuracy and confidence in the use of the FFM for RLPs in variable amplitude loading conditions using the equivalent cycles method, a statistical analysis similar to that discussed previously was performed. In addition to the uncertainties in damage growth rate measurement, the uncertainties in the loading conditions and Paris exponent now have to be considered. The relative change in loading is assumed to have a mean of 20%

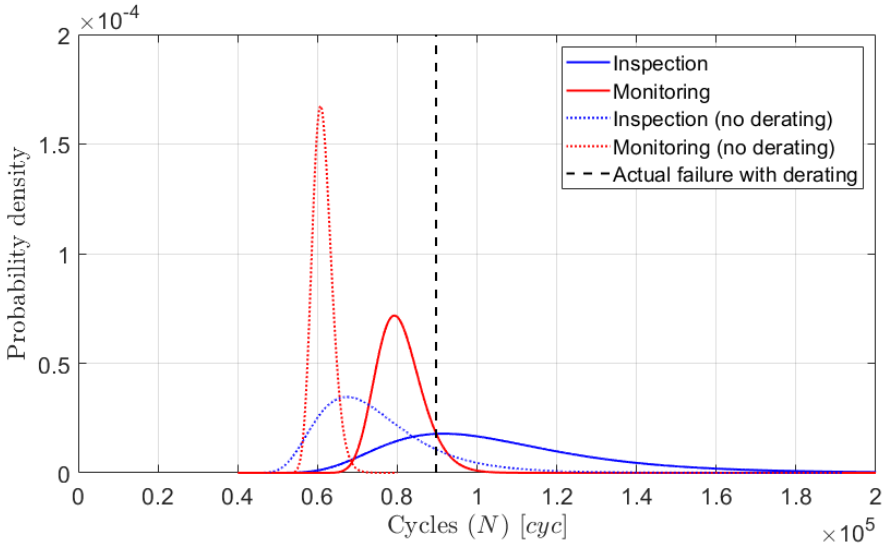

Figure 16: Plot of PDF of the predicted failure prior to the change in loading. The blue and red graph represents the inspection and monitoring approaches respectively. The dotted graphs represent the original predictions assuming that the component will not be derated. The solid line graphs represent the estimates assuming the component would be derated. The black line is when the component failed.

and a standard error of 2%. The uncertainty in the Paris exponent is not considered in BS7910. Therefore in this analysis, the Paris exponent is assumed to have a mean of $m = 2.88$ and a coefficient of variation, $COV = 0.0582$. The mean value is from the BS7910, while the COV was obtained from the statistical analysis by Gobbato [14] of the Virkler fatigue test data [5]. For comparison, a statistical analysis was also performed for the periodic inspection case with the same uncertainties shown earlier in Table 2.

Figure 16 shows the results of the analysis. The dotted lines show the probability density functions of the remnant life estimation assuming the original loading conditions; of course these predictions underestimate the failure time as the true remnant life was extended by the derating. The corrected remnant life estimates based on the assumed change in load is shown in Figure 16 with solid lines. As with the constant load results of Fig 10, the uncertainty in the life prediction made with the FFM is lower than that from the inspection based approach. However, the improvement is not as large as the constant amplitude loading results as in order to account for variable amplitude loading, the FFM now relies on the relative change in loading conditions and the Paris exponent, each with associated uncertainty, which translates to less confident predictions.

It can be seen in Figure 16 that the FFM underestimates the remnant life after the change in loading. This underestimation is caused by crack growth retardation as a result of crack blunting, similar to the effect of a single overload [28]. Figure 15(c) shows that there is a sudden decrease in crack growth rate for the first few cycles after the load decreases. The initial cycles at high load create a comparatively larger plastic zone in front of the crack tip, which the initial cycles of the low load have to propagate through; this results in a decrease in crack growth rate and subsequently extends the life of the component beyond what would be predicted before derating.

A similar experiment with a 40% decrease in loading was conducted and this effect of crack growth retardation was even more severe, resulting in inaccurate RLPs. This further reinforces the conclusions made in section 4, that a change in damage accumulation mechanism would invalidate the RLPs made using the FFM. This is

also true with the inspection-based approach, where crack growth laws are invalidated when the crack growth characteristics are affected by the loading history of the component. Empirical compensations were developed to account for the effect [29, 30], but again more input parameters with uncertainties would have to be introduced, resulting in greater uncertainties in the RLPs made.

Once the component has operated for a period at the derated conditions, there is the option to disregard data from the previous loading conditions and restart the FFM prediction with only the data collected under the new loading conditions. It is evident from Figure 15 (c) that starting from approximately $6 \times 10^4 cycs$, the linear relation between inverse damage accumulation rate and number of cycles is restored and subsequent data can be used to perform RLPs using the standard FFM. What is shown with this equivalent cycle method is that the monitoring approach can more confidently predict the effect of changes in operating conditions on component life prior to the actual change than an inspection immediately before the derating.

6 Conclusions

The accuracy and uncertainty in remnant life predictions made using crack size measurements from conventional periodic inspection and damage growth rate based estimates from permanently installed monitoring have been compared on data from a fatigue test instrumented with a potential drop measurement system. The remnant life estimates obtained from the permanently installed monitoring system using the Failure Forecast Method provided more accurate remnant life predictions with much greater confidence than estimates from the conventional approach using crack length measurements and Paris Law. The smaller uncertainty in the estimates using the Failure Forecast Method is largely due to it being based simply on the rate of increase of the damage-related signal with no requirement for knowledge of the load or material constants.

The Failure Forecast Method using permanently installed monitoring can be modified to accommodate step changes in loading, but the load change must be measured and the relationship between load and crack growth rate must be known, so increasing the data requirements and the resulting uncertainty in the estimates. The results with both methods are invalidated if the change in loading results in a change in the damage accumulation mechanism.

The basic Failure Forecast Method assumes infinite damage growth rate at failure. The fitness-for-service criterion is sometimes the ability of the structure to withstand an extreme load, rather than integrity under normal loading. It has been discussed how the Failure Forecast Method can be adapted to deal with this case, but again at a cost of more information on material properties and loading conditions being required.

The study has shown that the frequent data obtained from permanently installed monitoring systems provides new opportunities in remnant life estimates and potentially opens the way to increasing the intervals between outages and reducing design conservatism.

7 Acknowledgements

This work was supported by the UK Engineering and Physical Sciences Research Council via the UK Research Centre in NDE, grant EP/L022125/1.

References

[1] F. Braithwaite, "On the fatigue and consequent fracture of metals," *ICE Minutes Proceedings*, vol. 13, pp. 463–474, 1854.

[2] A. Donald, "A cracking tale: why did the world's first jetliner fall out of the sky?," *The Guardian*, Jan 2013. [Online].

[3] O. Adedipe, F. Brennan, and A. Kolios, "Review of corrosion fatigue in offshore structures: Present status and challenges in the offshore wind sector," *Renewable and Sustainable Energy Reviews*, vol. 61, pp. 141–154, Aug 2016.

[4] O. C. Garrido, S. E. Shawish, and L. Cizelj, "Crack growth assessment in pipes under turbulent fluid ixing using an improved spectral loading approach and linear elastic fracture mechanics," in *25th International Conference Nuclear Energy for New Europe*, NENE, 2016.

[5] D. A. Virkler, B. M. Hillberry, and P. K. Goel, "The statistical nature of fatigue crack propagation," Tech. Rep. AFFDL-TR-78-43, Air Force Flight Dynamics Laboratory, 1979.

[6] "Assessing and modelling the uncertainty in fatigue crack growth in structural steels," RR643, Health and Safety Executive, 2008.

[7] K. Ortiz and A. S. Kiremidjian, "Stochastic modeling of fatigue crack growth," *Engineering Fracture Mechanics*, vol. 29, pp. 317–334, jan 1988.

[8] "Guide to methods for assessing the acceptability of flaws in metallic structures," BS 7910:2013+A1:2015, The British Standards Institution, 2015.

[9] "Probabilistic methods for planning of inspection for fatigue cracks in offshore structures," DNVGL-RP-C210, DNV GL, 2015.

[10] J. Rudolph and S. Bergholz, "The AREVA integrated and sustainable concept of fatigue design, monitoring and re-assessment," in *Volume 1: Codes and Standards*, ASME, 2008.

[11] E. P. Carden and P. Fanning, "Vibration based condition monitoring: A review," *Structural Health Monitoring: An International Journal*, vol. 3, pp. 355–377, dec 2004.

[12] Z. Bo, Z. Yanan, and C. Changzheng, "Acoustic emission detection of fatigue cracks in wind turbine blades based on blind deconvolution separation," *Fatigue & Fracture of Engineering Materials & Structures*, vol. 40, pp. 959–970, dec 2016.

[13] S. Jiao, L. Cheng, X. Li, P. Li, and H. Ding, "Monitoring fatigue cracks of a metal structure using an eddy current sensor," *EURASIP Journal on Wireless Communications and Networking*, vol. 2016, aug 2016.

[14] M. Gobbato, J. P. Conte, and J. B. Kosmatka, "Statistical performance assessment of an NDE-based SHM-DP methodology for the remaining fatigue life prediction of monitored structural components and systems," *Proceedings of the IEEE*, vol. 104, pp. 1575–1588, aug 2016.

[15] J. Corcoran, "Rate-based structural health monitoring using permanently installed sensors," *Proceedings of the Royal Society of London A: Mathematical, Physical and Engineering Sciences*, vol. 473, no. 2205, 2017.

[16] B. Voight, "A relation to describe rate-dependent material failure," *Science*, vol. 243, no. 4888, pp. 200–203, 1989.

[17] "Standard test method for measurement of fatigue crack growth rates," ASTM E647-15, ASTM International, 2016.

[18] M. D. Todd, M. Leung, and J. Corcoran, "A probability density function for uncertainty quantification in the failure forecast method," in *9th European Workshop on Structural Health Monitoring*, BINDT, Jul 2018.

[19] P. Paris and F. Erdogan, "A critical analysis of crack propagation laws," *Journal of Basic Engineering*, vol. 85, no. 4, pp. 528–533, 1963.

[20] N. A. Zentuti, J. D. Booker, R. A. W. Bradford, and C. E. Truman, "A review of probabilistic techniques: towards developing a probabilistic lifetime methodology in the creep regime," *Materials at High Temperatures*, vol. 34, pp. 333–341, sep 2017.

[21] "Information for the procurement and conduct of ndt, part 4: Ultrasonic sizing errors and their implication for defect assessment," , Health and Safety Executive, 2008.

[22] M. Moles, L. Wesley, and T. Sinclair, "Accurate defect sizing using phased array and signal processing," in *Developments in Ultrasonics Inspection II*, JRC NDE, 2009.

[23] B. Voight, "A method for prediction of volcanic eruptions," *Nature*, vol. 332, pp. 125–130, 1988.

[24] R. G. Forman, V. E. Kearney, and R. M. Engle, "Numerical analysis of crack propagation in cyclic-loaded structures," *Journal of Basic Engineering*, vol. 89, no. 3, p. 459, 1967.

[25] NASGRO Consortium, "Fatigue crack growth computer program NASGRO® version 3.0. user manual, jsc-22267b," *NASA Technical report*, 2001.

[26] B. Yeter, Y. Garbatov, and C. G. Soares, "Reliability of offshore wind turbine support structures subjected to extreme wave-induced loads and defects," in *Volume 3: Structures, Safety and Reliability*, ASME, jun 2016.

[27] H. O. Basquin, "The exponential law of endurance tests," vol. 10, pp. 625–630, American Society for Testing and Materials Proceedings, 1910.

[28] A. Ray and R. Patankar, "Fatigue crack growth under variable-amplitude loading: Part i - model formulation in state-space setting," *Applied Mathematical Modelling*, vol. 25, no. 11, pp. 979 – 994, 2001.

[29] O. E. Wheeler, "Spectrum loading and crack growth," *Journal of Basic Engineering*, vol. 94, no. 1, p. 181, 1972.

[30] J. Willenborg, R. M. Engle, and H. A. Wood, "A crack growth retardation model using an effective stress concept," Tech. Rep. AFFDL-TM-71-1-FBR, Air Force Flight Dynamics Laboratory, 1971.